Journal of Hydrology: Regional Studies 23 (2019) 100599

Contents lists available at ScienceDirect

Journal of Hydrology: Regional Studies

journal homepage: www.elsevier.com/locate/ejrh

Estimation of probable maximum precipitation at three provinces in Northeast Vietnam using historical data and future climate change scenarios

Le Thi Thanh Thuy[a,c], Seiki Kawagoe[a,*], Ranjan Sarukkalige[b]

[a] Faculty of Symbiotic Systems Science, Fukushima University, 1 Kanayagawa, Fukushima city, Fukushima, 960-1296, Japan
[b] School of Civil and Mechanical Engineering, Curtin University, Kent Street, Bentley, Perth, Western Australia, 6102, Australia
[c] Faculty of Water Resources Engineering, Thuy Loi University, 175 Tay Son, Dong Da, Hanoi, Viet Nam

ARTICLE INFO

Keywords:
PMP
Clausius clapeyron
RCP
GCM
Northeast Vietnam

ABSTRACT

Study region: In this study, three provinces in Northeast Vietnam including Bac Kan, Thai Nguyen, and Tuyen Quang are examined to determine the precipitation variation characteristics.
Study focus: The average yearly temperature during the last two decades in Northeast Vietnam has increased by 0.72 °C when compared to the period 1962–1990. The Clausius Clapeyron (CC) relation indicates that a warmer atmosphere can result in higher moisture-holding capacity; hence, there is the possibility of increased extreme rainfall with respect to the rise in temperature. We evaluate the relationship between the average 24-hour temperature and rainfall extremes using the binning method. The estimation of the 24-hour probable maximum precipitation (PMP) is then implemented based on the moisture maximization and Hershfield statistical methods.
New hydrological insights for the region: The 99.9th percentiles of 24-hour precipitation are close to the super CC scaling up to peak points of 22.6–25.6 °C and decrease at higher temperatures. The Hershfield method produces 24-hour PMP results ranging from 232 mm to 895 mm. PMP outputs using the moisture maximization method based on the 100-year dew point are higher than those results generated from the statistical method except for Chiem Hoa station. Considering possible changes in future relative humidity under a warming climate from GCMs and RCM projections for two RCP scenarios, RCP 8.5 indicates the possible rise in probable extreme precipitation.

1. Introduction

Lying within the Southeast Asian typhoon belt, Vietnam experiences high frequencies of storms and heavy rainfall. Two obvious consequences of such extreme rainfalls are floods and landslides. In Vietnam, the Northeast region is considered one of the areas that is the most prone to such disasters and increases in frequency and intensity of heavy rainfall events in a warming climate (Le et al., 2014). Climate change does have great impacts on extreme precipitation events and should be taken into consideration (Hardwick Jones et al., 2010; Utsumi et al., 2011; Jakob and Walland, 2016). Within the context of global temperature change, extremely high precipitation intensities have been observed, highlighting a relationship between extreme rainfall and air temperature (Berg and Haerter, 2013; Panthou et al., 2014; Toure Halimatou et al., 2017; Herath et al., 2018). Such extreme rainfall events have also been estimated using probable maximum precipitation (PMP) (Beauchamp et al., 2013; Rousseau et al., 2014; Lee et al., 2016, 2017;

* Corresponding author.
E-mail addresses: lethanhthuy@tlu.edu.vn (L.T. Thanh Thuy), Kawagoe@sss.fukushima-u.ac.jp (S. Kawagoe), P.Sarukkalige@curtin.edu.au (R. Sarukkalige).

https://doi.org/10.1016/j.ejrh.2019.100599
Received 2 August 2018; Received in revised form 26 February 2019; Accepted 27 February 2019
Available online 16 March 2019

Rastogi et al., 2017).

Theoretically, PMP is defined by the World Meteorological Organization (WMO, 2009a) as "the greatest depth of precipitation for a given duration meteorologically possible for a design watershed or given storm area at a particular location at a particular time of year, with no allowance made for long-term climatic trends". Normally, PMP is used to determine probable maximum flood (PMF) for the design of hydraulic structures. The moisture maximization method (Beauchamp et al., 2013; Rousseau et al., 2014; Lee et al., 2016, 2017) and the Hershfield method (Hershfield, 1961, 1965; Casas et al., 2011; Jothityangkoon et al., 2013; Alias et al., 2013) represent two of the most widely used approaches in PMP estimation. The statistical method, which was developed by Hershfield, focuses on the frequency analysis and the influence of outliers on the mean and standard deviation of observed series of annual maxima at the location of interest (WMO, 2009; Micovic et al., 2015). The moisture maximization method considers the maximization ratio, which is the ratio between maximum precipitable water at a certain period of the year and actual precipitable water during a storm of interest. Precipitable water means the total amount of vapor water in the atmospheric column. In the case of unavailable radiosonde data, the surface dew point is used under the assumption of a saturated pseudo-adiabatic atmosphere. The maximum precipitable water can be estimated from the 100-year value or maximum observed value at a certain time window (WMO, 2009; Beauchamp et al., 2013; Rousseau et al., 2014).

Under the influence of a changing climate, temperature increases are believed to drive the higher intensity of precipitation in many areas in the world (Jones et al., 2010; Jakob and Walland, 2016; Herath et al., 2018). Such projection is mainly based on the hypothesis that the increase in water holding capacity of the atmosphere is associated with the rise in air temperature as described by the Clausius Clapeyron (CC) relationship (Utsumi et al., 2011). Assessments of temperature-precipitation scaling are often implemented using a binning technique in order to determine precipitation event scale properties (Herath et al., 2018). Many studies pointed out that the scaling between temperature and extreme precipitation has a close relationship with rainfall percentile, rain duration, time scale, and geographic location (Jakob and Walland, 2016; Boessenkool et al., 2016; Herath et al., 2018). For example, Hardwick Jones et al. (2010) concluded that the scaling relationship depends on rainfall percentile. In other words, the CC-scaling theory is mainly based on extreme events rather than average ones. Studies about convective precipitation have shown a super-CC scaling of about 14–15% per degree Celsius at higher temperatures (Berg et al., 2013; Berg and Haerter, 2013), while a CC-like scaling (6–7% per degree Celsius) was found at lower temperatures. Similar findings were also illustrated for a daily resolution (Utsumi et al., 2011; Berg and Haerter, 2013). In addition, based on geographic region, there are three major categories of the 99th percentile of 24-hour precipitation changes with temperature, namely monotonic increase, monotonic decrease, and a peak-like structure (Utsumi et al., 2011). The fifth IPCC report also showed that future air temperature and humidity are expected to gradually increase (IPCC, 2015; Jakob and Walland, 2016). Thus, climate change will have a strong impact on moisture maximization and PMP as a result. Recent studies have suggested that PMP is likely to rise in most areas of the world under a warmer climate (Beauchamp et al., 2013; Rousseau et al., 2014; Lee et al., 2016, 2017; Rastogi et al., 2017). Though most developed countries have well maintained long-term hydro-climatic data, difficulties in data availability are always a major issue hindering many studies in developing nations such as Vietnam.

Climate change is expected to increase the Northeast region's vulnerability through increasing temperature and erratic precipitation; abnormal rain, which was difficult to anticipate in terms of intensity, time, and place, has occurred more frequently in recent years (MONRE, 2016). In addition, the magnitudes of the maximum precipitable water could rise with increasing air temperature and thus could magnify extreme rainfall in the future (Kunkel et al., 2013; Ishida et al., 2018). Therefore, it is important to understand the precipitation variation characteristics in Northeast Vietnam, especially in a warming climate. Taking these facts into account, the main aims of this paper are to (i) identify the relationship between extreme 24-hour precipitation and average 24-hour temperature, (ii) estimate 24-hour PMPs in the study area, and (iii) evaluate the possible impacts of a warming climate on extreme precipitation and PMP.

2. Study area and data

2.1. Study area

In this paper, we examine the precipitation characteristics of three provinces in Northeast Vietnam, namely Bac Kan (BK), Thai Nguyen (TN), and Tuyen Quang (TQ) (Fig. 1). This area is covered by a mixture of mountainous and hilly terrain landscapes. During the period of 1960 to 2016, the average annual rainfall in this area was 1380–1900 mm. The rainy season often spans from May to October, with average monthly rainfall and average monthly temperature of 108–317 mm and 23.8–26.9 °C, respectively. The highest 24-hour precipitation in each month varies from 255 mm (May) to 506 mm (July) and from 375 mm to 231 mm in the remaining three months.

In addition, the largest 24-hour precipitation at 14 out of 18 rain stations coincided with typhoon-related events. According to historical typhoon data from NOAA (Chu et al., 2017), about 68 tropical cyclones in North Vietnam occurred from 1960 to 2016. Heavy rainfall in this area is not only a result of troughs and tropical concentration lines across the delta, but typhoon-related events that hit inland of Vietnam and South China as well. For example, due to the influence of Typhoon Bilis in 2006 in South China, the greatest 24-hour precipitation (*Rmax*) occurred at Cho Ra (CR_ 211 mm), Chiem Hoa (CH_506 mm), Ham Yen (HY_ 338 mm), and Tuyen Quang (TQ_ 316 mm). This typhoon also led to heavy rainfall (166–341 mm/day) at five rain gauge stations in Bac Kan province. Typhoons, which hit inland Vietnam, could lead to heavy rainfall in a larger region in each province of the study area. For instance, Typhoon Durian in 2001 brought heavy precipitation to six rain stations in Thai Nguyen (208–349 mm/day) and five rain stations in Tuyen Quang (160–361 mm/day). Typhoon Noname in 1986 also led to heavy precipitation (150–229 mm/day) at five

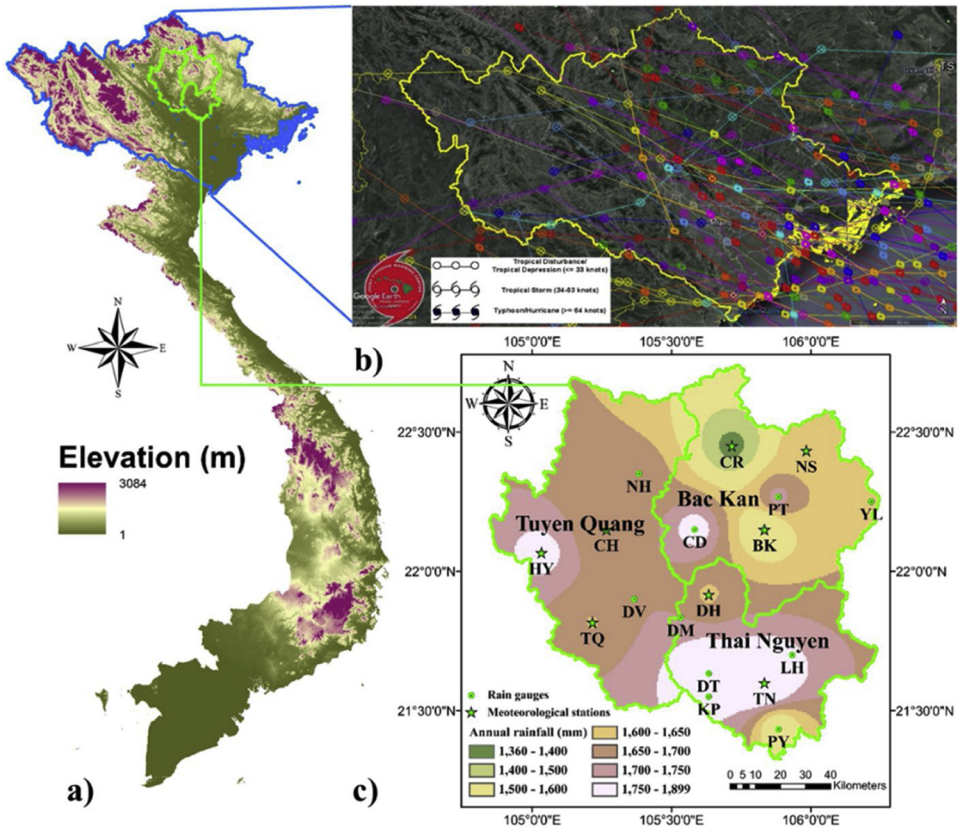

Fig. 1. a) Elevation distribution in Vietnam; b) Typhoons, storms and tropical depressions in North Vietnam 1960–2016 (Chu et al., 2017); c) Average annual rainfall in study area.1960–2016.

stations in Bac Kan. Troughs (low atmospheric pressure), or tropical concentration lines showed rare magnitudes of 24-hour precipitations (*Rmax*) at Dinh Hoa (DH_ 276 mm), Thai Nguyen (TN_375 mm), Bac Kan (BK_305 mm), and Ngan Son (NS_260 mm).

2.2. Hydro-meteorological data

In Bac Kan, Thai Nguyen and Tuyen Quang provinces, there are eight meteorological stations and 34 rain gauge stations, 21 stations of which were constructed before 2006. Many rain gauges have discontinuous data (meaning they record only some rainy months of the year or have missing data for years or months), short length data (recent construction stations), or are manually measured by local people. Stations including BK, CR, NS, DH, TN, CH, HY, and TQ have been measuring surface meteorological parameters such as precipitation (*R*), temperature (*t*), and relative humidity (*RH*) since 1962 (Table 1). In this paper, we, therefore, utilized the average 24-hour data of *R*, *t*, and *RH* from 1962 to 2016 from eight meteorological stations to evaluate the characteristics of precipitation.

To evaluate the spatial distribution of storm rainfall as a function of storm duration, the Depth-Area-Duration (DAD) curve is often established (WMO, 1969). In this study, we selected heavy storm events to envelop a depth-area curve of the 24-hour

rainstorm (WMO, 1969, 2009a) based on the Thiessen polygon weighting method in addition to Inverse Distance Weight (IDW) interpolation (WMO, 1969; Shin et al., 2013), as represented in Fig. 2.

Climate data, that is, daily temperature data, were obtained from the World Climate Research Programme – CMIP5 (https://esgf-node.llnl.gov/projects/cmip5/) for GCMs, and the Coordinated Regional Climate Downscaling Experiment – CORDEX in the East Asia region for RCMs. The specification of each model is shown in Table 2. Using the Climate Data Operators (CDO) program (Schulzweida, 2018), we evaluated two Global Climate Models from Japan, including MIROC 5 (MIR) (Watanabe et al., 2010) and MRI-CGCM3 (MRI) (Yukimoto et al., 2012), and one Regional Climate Model, namely HadGEM3-RA (HaG) (Baek et al., 2013; Davies et al., 2005). RCP4.5 (stabilization scenario) and RCP8.5 (pessimistic emission scenario) were considered regarding two time periods: 2050 (2021–2050) and 2080 (2051–2080).

3. Methodology

In order to evaluate the behavior of extreme precipitation in a changing climate, we analyzed the relationship between

Table 1
Main characteristics of weather stations in the study area.

No	Province	Station		Elevation (m)	Type of station	Parameters	Observation time steps	Period of record
1	Bac Kan	Bac Kan	BK	145	MS2[a]	*R* [e], *RH* [f], *t* [g]	6 h 1 h	1957-2016 1962-2016
2	Bac Kan	Cho Ra	CR	165	MS3[b]	*R, RH, t*	6 h 1 h	1962-2016 1964-2016
3	Bac Kan	Ngan Son	NS	650	MS3	*R, RH, t*	6 h 1 h	1962-2016 2003-2016
4	Bac Kan	Cho Don	CD	503	RG[c]	*R*	6 h	1961-2016
5	Bac Kan	Phu Thong	PT	202	RG	*R*	6 h	1980-2016
6	Thai Nguyen	Dinh Hoa	DH	105	MS1[d]	*R, RH, t*	6 h 1 h	1961-2016 1965-2016
7	Thai Nguyen	Thai Nguyen	TN	40	MS1	*R, RH, t*	6 h 1 h	1959-2016 1959-2016
8	Thai Nguyen	Ky Phu	KP	122	RG	*R*	6 h	1961-2016
9	Thai Nguyen	Dai Tu	DT	70	RG	*R*	6 h 1 h	1959-2016 1972-1982
10	Thai Nguyen	Pho Yen	PY	14	RG	*R*	6 h	1997-2016
11	Tuyen Quang	Chiem Hoa	CH	60	MS3	*R, RH, t*	6 h 1 h	1962-2016 1962-2016
12	Tuyen Quang	Ham Yen	HY	50	MS3	*R, RH, t*	6 h 1 h	1962-2016 1973-2016
13	Tuyen Quang	Tuyen Quang	TQ	50	MS1	*R, RH, t*	6 h 1 h	1960-2016 1960-2016
14	Tuyen Quang	Na Hang	NH	70	RG	*R*	6 h	1963-2016
15	Tuyen Quang	Dao Vien	DV	550	RG	*R*	6 h	1997-2016

[a] Meteorological station – Class II.
[b] Meteorological station – Class III.
[c] Rain gauge station.
[d] Meteorological station – Class I.
[e] Rainfall.
[f] Relative humidity.
[g] Temperature.

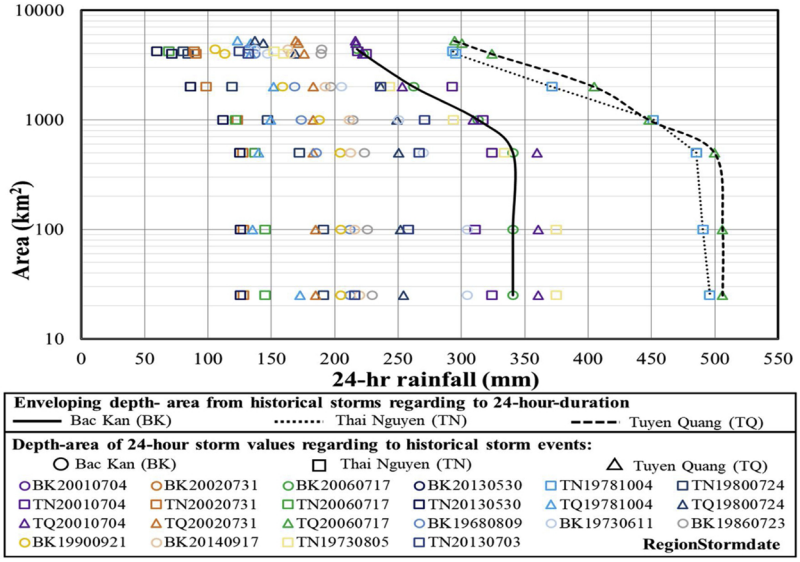

Fig. 2. Depth-area envelope of the 24-hour rainstorm at three regions (Bac Kan (BK), Thai Nguyen (TN), and Tuyen Quang (TQ)) based on heavy storms data from 1962 to 2016.

temperature and extreme rainfall during the rainy season. The Probable Maximum Precipitation (PMP) was then estimated using historical meteorological data. For simplification, we estimated the possible changes in relative humidity at high temperatures based on historical data and considered the changes in projected temperature (Global Climate Models – GCMs and Regional Climate Model - RCM) and relative humidity in order to evaluate the extent of changes in PMP under climate change condition. The method developed in the present study is described in Fig. 3.

3.1. Precipitation and temperature scaling analysis

It is important to understand the relationship between extreme precipitation and one of its related meteorological variable: atmospheric temperature, especially under changing climate conditions. The binning technique has been widely applied to evaluate such a relationship between temperature and precipitation (*t-R*) (Hardwick Jones et al., 2010; Lenderink et al., 2010; Utsumi et al., 2011; Herath et al., 2018). Based on recent literature, two main approaches in the (*t-R*) analysis include the same bin width and the

Table 2
Specification of climate models.

Category	Model name	Code	Resolution Latitude × Longitude	Scenarios	Source
GCM	Model for Interdisciplinary Research On Climate version 5 (MIROC5)	MIR	1.4008 ° × 1.40625°	RCP2.6 RCP4.5 RCP6.0 RCP8.5	http://cmip-pcmdi.llnl.gov/cmip5/
	Meteorological Research Institute Couple Global Climate Model version three (MRI-CGCM3)	MRI	1.12148° × 1.125 °	RCP2.6 RCP4.5 RCP6.0 RCP8.5	http://cmip-pcmdi.llnl.gov/cmip5/
RCM	Hadley Centre Global Environment Model, version 3 Regional climate model (HadGEM3-RA)	HaG	0.44° × 0.44°	RCP4.5 RCP8.5	http://cordex-ea.climate.go.kr/cordex/

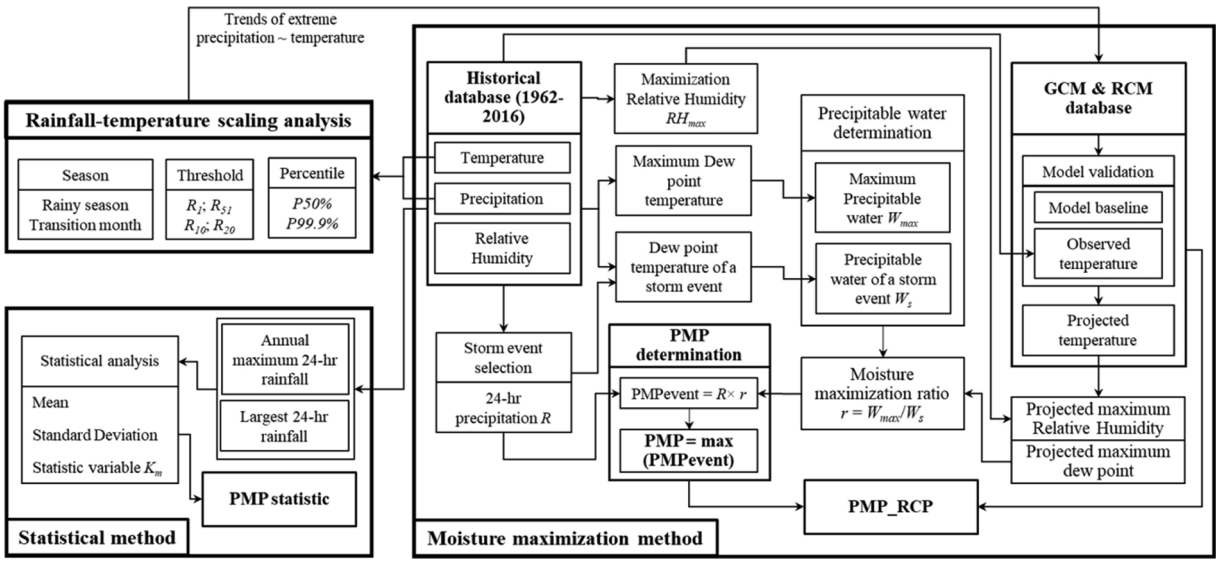

Fig. 3. Illustration of the proposed methodology in analysing rainfall-temperature scaling and computing PMPs relation to the statistical and moisture maximization methods.

same number of samples in each temperature bin. In the former method, precipitation is paired with temperature with an equal width such as 1 °C (Berg et al., 2013). Since the utilization of even-width bin sometimes leads to fewer samples in some bins, especially in lower and upper-temperature ranges (Hardwick Jones et al., 2010), the equal-bin width method with adjustment to assure a given minimum of samples in each bin offers an interesting alternative. For example, Utsumi et al. (2011) used the 2 °C bin with minimum samples of 150 for the global study; Berg et al. (2009) defined the minimum samples of 300 for each bin width in their study of the entire European domain. In the latter method, (*t-R)* pairs are placed in each bin in order to have the same sample size regardless of the bin width (for example 233 events per one bin in a research of Hardwick Jones et al., 2010). However, it is sometimes difficult to obtain the same sample size within each of the smallest temperature bins (e.g., 0.1 °C).

To determine the behavior of extreme precipitation, we set up a relationship between 24-hour rainfall and average 24-hour air surface temperature for wet events, which have been defined differently in various studies. According to the World Meteorological Organization guidelines (WMO, 2009b), precipitation depths with a threshold of 1 mm, 10 mm and 20 mm are set for wet day events (R_1), heavy precipitation (R_{10}), and very heavy precipitation (R_{20}), respectively. For a given rainfall duration, wet day events were also set as 0.3 mm (Herath et al., 2018), 0.1 mm (Hardwick Jones et al., 2010), 0.3 mm/hour (Panthou et al., 2014), or 20 mm (Toure Halimatou et al., 2017). In the Vietnamese government standard (Vietnam Standard, 2015), the 24-hour rainfall amount from 51 mm and above (R_{51}) is considered a rain-induced waterlogging event. In addition, the WMO guideline (WMO, 2009b) indicates that the 95th percentile of precipitation (P_{95}) on wet days is used to determine a very wet day event, while an extremely wet day event is calculated from the 99th percentile of precipitation (P_{99}). Recent studies have applied the 50th (Hardwick Jones et al., 2010; Herath et al., 2018), 75th (Berg and Haerter, 2013), 90th (Panthou et al., 2014), 99th (Utsumi et al., 2011), or 99.9th (Lenderink et al., 2011) percentiles of precipitation for given rainfall duration in the (*t-R*) scaling analysis.

In this study, we evaluated the behavior of the 99.9th percentile precipitation ($P_{99.9}$) on wet days (R_1) and heavy rain days (R_{51}) of the rainy season (May – October) at eight meteorological stations from 1962 to 2016. During this period, the total number of wet days (R_1) and heavy rain days (R_{51}) at eight stations were 32,243 and 2579 for temperature ranges of 13.8–38 °C and 16.6–30.7 °C, respectively. Fig. 4. a) illustrates the number of days in each temperature bin width of 1 °C. Since there were great differences between sample sizes in each bin width, pairs of average 24-hour temperature and rainfall were allocated in each bin width of 1 °C more or less to ensure a given minimum number of samples in each bin, such as 150 (R_1) and 50 (R_{51}) for the whole study region. The CC scaling was used to examine the possible changes in the precipitation as a function of changes in temperature. The exponential regression was applied to determine precipitation ($P_{t+\Delta t}$) that related to changes in temperature (Δt) (Hardwick Jones et al., 2010), as described in Eq. (1):

$$P_{t+\Delta t} = P_t(1 + \alpha)^{\Delta t} \quad (1)$$

where t is air temperature (°C); Δt refers to the rise in temperature (°C); P_t and $P_{t+\Delta t}$ denote rainfall at air temperature t and $t+\Delta t$, respectively (mm); and α represents the rate at which precipitation changes with temperature. For example, $\alpha = 0.07019$ and $\alpha = 0.0607$ are equivalent to CC scaling of 7.019% per degree Celsius at 4 °C and 6.007% per degree Celsius at 24 °C, respectively.

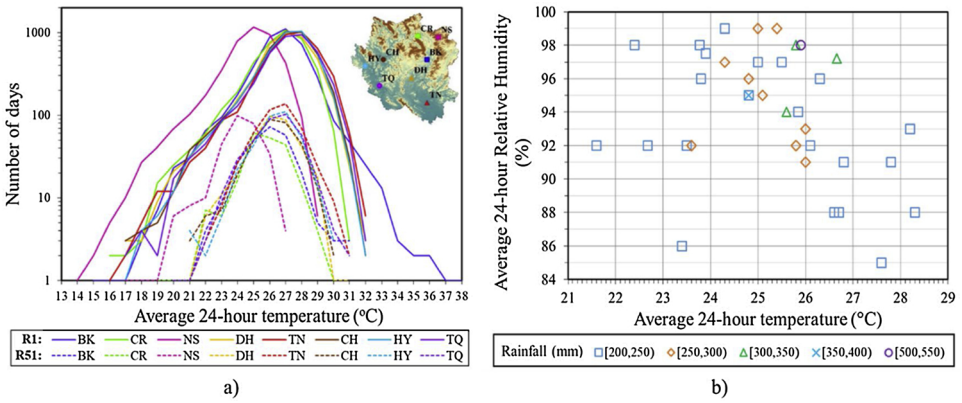

Fig. 4. a) Temperature distribution curve in rainy season (May-October) at each station over 55 years (1962–2016) with regard to wet event (R_1) (solid lines) and rain-induce water logging events (R_{51}) (dot lines); b) Relationship between Relative Humidity and temperature (*RH- t*) with respect to extreme 24-hour rainfall classification at the study site.

3.2. Estimation of the PMP

3.2.1. The statistical method

This approach applies the Hershfield method (1961) to estimate the PMP (WMO, 2009a), as described in Eq.(2):

$$PMP = \bar{R}_n + S_n \times K_m = \bar{R}_n + S_n \frac{R_{max} - \bar{R}_{n-1}}{S_{n-1}} \tag{2}$$

where PMP is probable maximum precipitation (mm); $\bar{R}$ and S are in mm, representing mean and standard deviation. Sub-index (n) and (n-1) refer to annual extreme series and annual extreme series excluding the largest value, respectively. *Rmax* is the maximum rainfall in the series (mm); K_m substitutes for the statistical variable, which represents the maximum value within the observed series of storm events.

3.2.2. The maximization method

This method considers the maximization ratio between maximum precipitable water (*Wmax*) at a certain period of the year and actual precipitable water (W_s) of the storm event associated with precipitation R (mm), as described in Eq.(3).

$$PMP = R \frac{W_{max}}{W_s} \tag{3}$$

where W_s refers to precipitable water estimated for the storm (mm) and *Wmax* represents the maximum precipitation water indicated for the storm reference location (mm). In addition to station elevation, dew point temperature the day of storm occurrence (t_d) is used to determine W_s. *Wmax* is also computed regarding location of station and maximum dew point temperature ($t_d max$), which can be taken as the 100-year return period (t_{d_100}) of maximum dew point in the month of the storm occurrence. It also can be maximum dew point within 15 days (t_{d_15d}) (15 days after the storm event), within a 30-day window (t_{d_30d}) (15 days before and 15 days after the storm), or the largest value of $t_d max$ series in a month of the storm event (t_{d_month}) (WMO, 2009a; Lee et al., 2016).

In practice, after selecting extreme rainfall events, precipitable waters were determined using annex 1 of the WMO manual on the estimation of PMP (WMO, 2009a), taking station elevation and surface dew point temperature (t_d) into consideration. Normally, a persisting 12-hour dew point temperature is used for storm maximization. According to the WMO manual, a 24-hour interval can be used for longer storm duration in some tropical areas to select historical maximum dew points and representative dew points of storms (WMO, 2009a). The application of the 24-hour dewpoint for adjusting storm rainfall can be an alternative in PMP calculation as it provides few differences from the application of the 12-hour representative storm dew point. In case the t_d record is unavailable, an average 24- hour surface dew point temperature is estimated based on the average 24-hour relative humidity (*RH*) and surface temperature (t), as described in Eq. (4) (Alduchov and Eskridge, 1996; Lawrence and Planck, 2005)

$$t_d = \frac{243.04 \times \left(\ln \frac{RH}{100} + \frac{17.625 \times t}{243.04 + t}\right)}{17.625 - \ln \frac{RH}{100} - \frac{17.625 \times t}{243.04 + t}} \tag{4}$$

where t_d refers to dew point temperature (°C); *RH* represents relative humidity (%); and t is surface temperature (°C).

3.3. PMP and climate change

As mentioned in Section 3.2.2, the determination of *Wmax*, which often depends on the elevation of observation location, temperature, and relative humidity, has a critically important role in PMP calculation. Because raw climate model data often has a

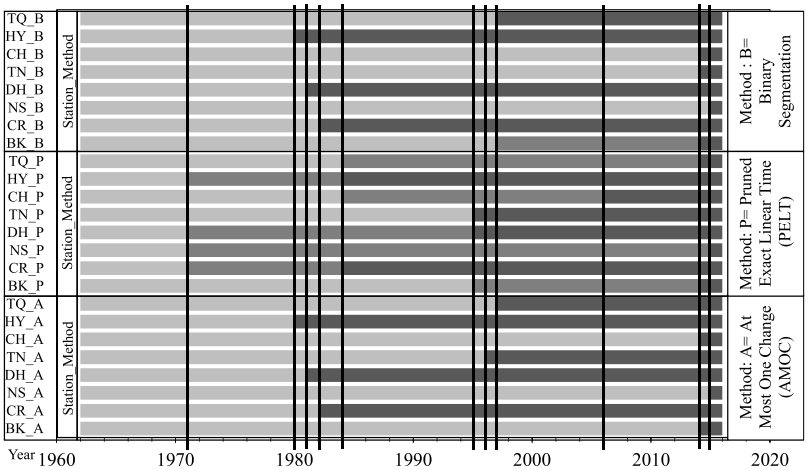

Fig. 5. Identifying changes in mean value for average monthly temperature data in the rainy season (May – October) at eight stations from 1962–2016 regard to three methods: At Most One Change (A), Pruned Exact Linear Time (P), and Binary Segmentation (B). Vertical black lines represent changing points; the coloured bars (light grey, grey, and dark grey) indicate ranges of years obtaining relatively stable conditions in mean value.

significant bias, correction for a specific study site is therefore necessary. The adjustment of climatic model simulations can be implemented by bias correction methods, including linear scaling, local intensity scaling, variance scaling, distribution scaling, power transformation, or distribution mapping (Terink et al., 2009, 2010; Teutschbein and Seibert, 2012; Chen et al., 2013; Fang et al., 2015). While precipitation changes are often evaluated using a ratio of future to historical data, changes in temperature are often estimated based on the difference between the future and historical data (Pierce et al., 2015). Being considered as an approximately normally distributed variable, the temperature is often corrected through its mean and variance using the variance scaling method (Terink et al., 2010; Teutschbein and Seibert, 2012; Hawkins et al., 2013; Fang et al., 2015). In this approach, it is assumed that bias correction would be stationary. This means that the current correction parameters are valid in future cases (Teutschbein and Seibert, 2012; Pierce et al., 2015).

Using R package (Killick and Eckley, 2013, 2016), we implemented a change point analysis to identify changes in mean for monthly temperature data in the rainy season at eight stations in regard to three methods: AMOC (at most one change), PELT (pruned exact linear time), and BinSeg (binary segmentation). In general, the mean values of monthly temperature from May–October in this study site experienced change points within a 10-year period (Fig. 5 & Table 3). In addition, according to the Guidelines on the Calculation of Climate Normals (WMO, 2017), the standard normal can be applied to assess climatological surface parameters such as air surface temperature. The basic assumption of a stationary climate assumes that the climate is variable; however, the variations properties are considered to be constant with time (WMO, 2017). With respect to Teutschbein and Seibert (2012), the procedures of bias correction utilized a transformation algorithm in order to adjust the output of GCMs and RCM and to identify possible biases between observation and simulation data. In addition, the major contributor to differences between observed data and model output are considered as a bias correction, rather than climatic differences between two time periods (Teutschbein and Seibert, 2012; Pierce et al., 2015).

According to WMO guidelines (WMO, 2017), “normals” refer to an average computational time for “a uniform and relatively long period” covering “at least three consecutive ten-year periods”. In this paper, we therefore apply the variance scaling method to correct temperature series for 30-year periods including 1971–2000 for historical records (*H*) and 2021–2050 and 2051–2080 for future (*F*) projections with respect to observations (*O*) and climate models output (*M*). The corrected daily future temperature (T_F) on a j^{th} day (*d*) of an i^{th} month (*m*) is calculated based on the relationship between mean ($\bar{T}$) and standard deviation (*S*) of monthly temperature from historical observation (*O_H*) and historical simulation (*M_H*), as indicated in Eq. (5).

$$T_{F,m_i,d_j} = \bar{T}_{O\_H,m_i} + \frac{S_{O\_H,m_i}}{S_{M\_H,m_i}} \times (T_{M\_F,m_i,d_j} - \bar{T}_{M\_H,m_i}) \quad (5)$$

where T_{F,m_i,d_j} represents the corrected daily future temperature (°C) on the j^{th} day of the i^{th} month; $\bar{T}_{O\_H,m_i}$ and $\bar{T}_{M\_H,m_i}$ denote mean the monthly temperature (°C) in the i^{th} month (m_i) of historical observation data (*O_H*) and historical data of model output (*M_H*), respectively. S_{O_H,m_i} and S_{M_H,m_i} illustrate the standard deviation of monthly temperature (°C) in the i^{th} month of historical observation and historical model output, respectively. T_{M_F,m_i,d_j} refers to the future temperature (°C) obtained from the climate models projection on the j^{th} day of the i^{th} month.

Regarding the projected temperature for each climate model, the maximum *RH* (*RHmax*) was estimated based on the analysis of historical temperature and *RH* (*f˜RH*) using the binning method. Relative humidity was paired with temperature using the equal-bin width of 0.1 °C. The largest value of *RH* within each bin was defined as the maximum magnitude of relative humidity (*RHmax*) at that temperature. The upper boundary of *RHmax* at high temperature was then identified to evaluate possible maximum relative humidity

Table 3
Identifying changes in mean value for average monthly temperature data in the rainy season (May – October) at eight stations (BK, CR, NS, DH, TN, CH, HY, and TQ) from 1962 to 2016 in regard to three methods At Most One Change (AMOC), Pruned Exact Linear Time (PELT), and Binary Segmentation (BinSeg). Black lines present the average monthly temperature in the rainy season at each station from 1962 to 2016. Horizontal red lines represent the mean value of monthly temperatures within each stable period.

	Methods		
	AMOC	BinSeg	PELT
BK	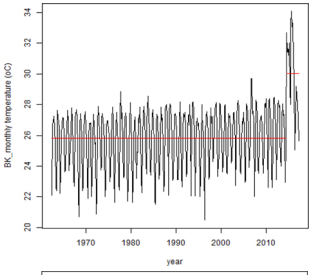	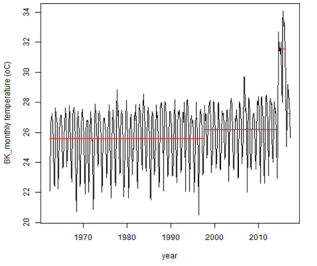	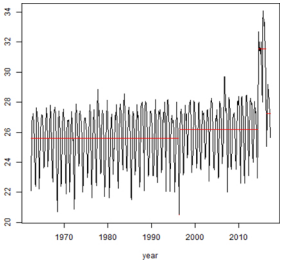
CR	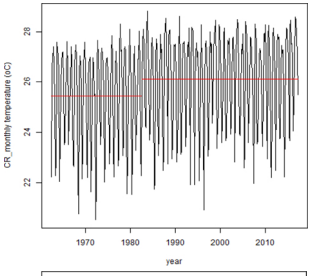	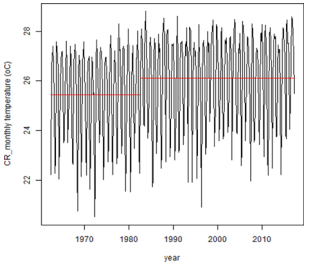	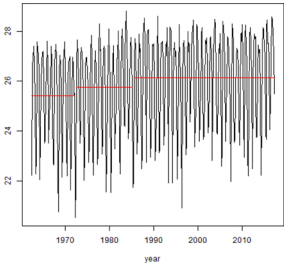
NS	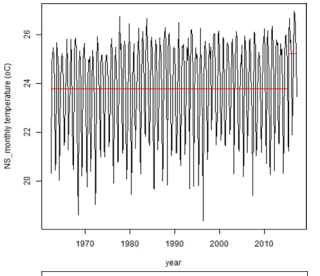	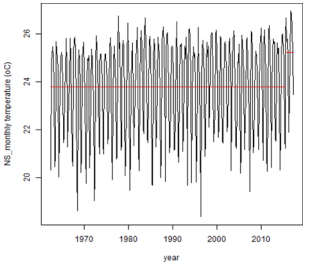	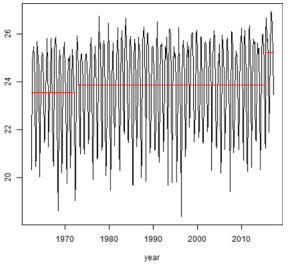
DH	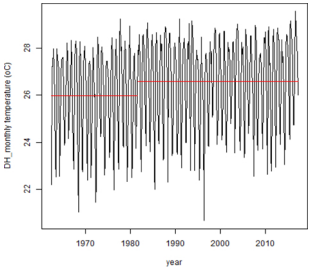	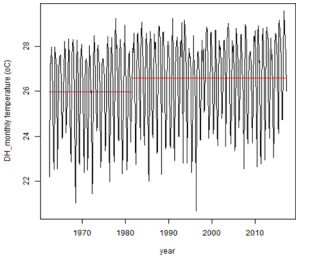	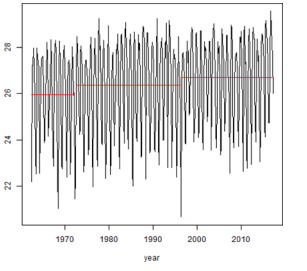

(*continued on next page*)

Table 3 (*continued*)

	Methods		
	AMOC	BinSeg	PELT
TN	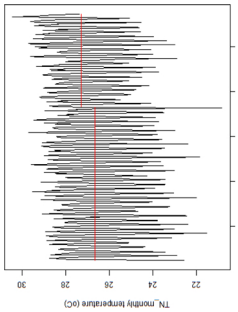	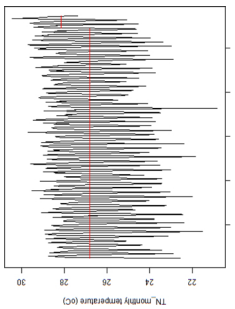	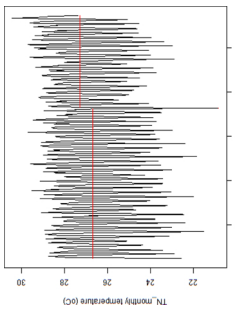
CH	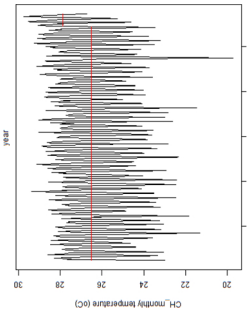	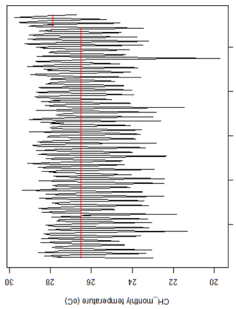	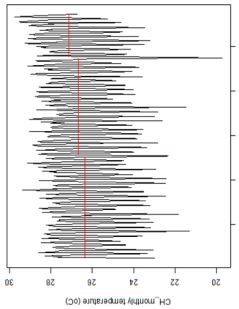
HY	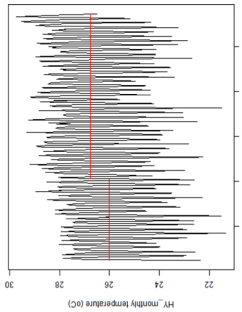	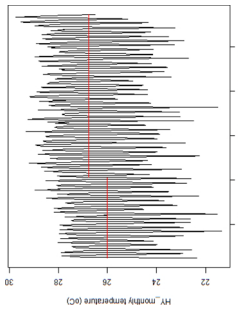	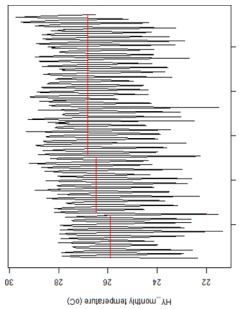
TQ	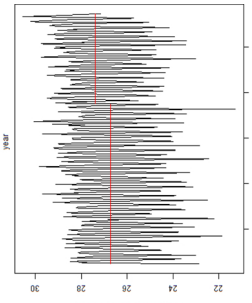	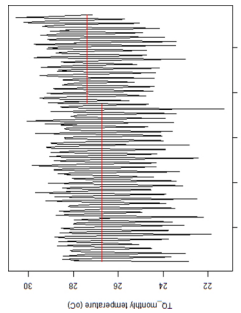	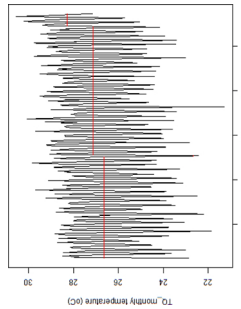

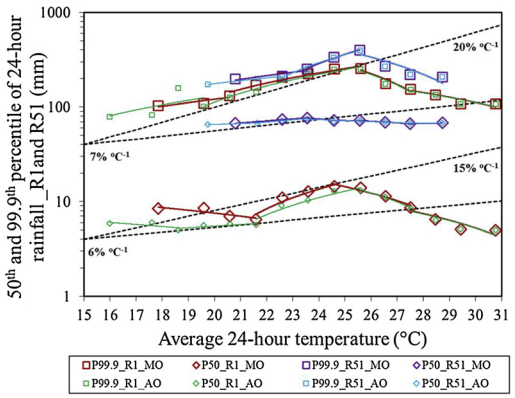

Fig. 6. Rainfall and temperature scaling analysis at study region (all 8 stations) for 99.9th ($P_{99.9}$) and 50th (P_{50}) percentiles of wet events (R_1), heavy precipitation (R_{10}), very heavy precipitation (R_{20}), and rain-induced waterlogging event (R_{51}) from May – October ($P_{99.9\_R1\_MO}$, $P_{50\_R1\_MO}$, $P_{99.9\_R51\_MO}$ and $P_{50\_R51\_MO}$), and from April – October (($P_{99.9\_R1\_AO}$, $P_{50\_R1\_AO}$, $P_{99.9\_R51\_AO}$ and $P_{50\_R51\_AO}$). The linear regressions within temperature ranges are shown in solid lines; the scaling rates are represented by dot black lines.

based on projected temperature. The possible maximum dew points were then computed in accordance with future projected temperatures for each GCM_RCP and RCM_RCP in order to determine the possible *Wmax* and PMP in a future month.

4. Result

4.1. Precipitation and temperature scaling analysis

In general, the 99.9th percentile of two datasets (R_{51} and R_1) at all stations in the rainy season from May to October (MO) are associated with a peak point temperature of about 26 °C, then they decrease at higher temperatures (Fig. 6). The CC-like relation with the rate of 7% per degree Celsius almost fits the rise of $P_{99.9\_R51\_MO}$ between 20.8 °C and 22.6 °C. Significant increases in extreme precipitation to the peak point temperature demonstrates super CC rates of 15–20% per degree Celsius between 22.6 °C and 25.6 °C for $P_{99\_R51\_MO}$, $P_{99\_R1\_MO}$, and $P_{50\_R1\_MO}$. The decrease of extreme precipitation intensities at high temperature would be associated with the decline of relative humidity (Hardwick Jones et al., 2010; Utsumi et al., 2011).

Regarding (*t-R*) analysis at each station, the scaling rate of the 50th percentile of R_{51} agrees with CC-like scale from 7% per degree Celsius (NS, DH, TN, and TQ) to 10% per degree Celsius (CR, CH), and 20% per degree Celsius (BK, HY). The super CC scaling rates of more or less than 20% per degree Celsius are shown for the three lines: $P_{99.9\_R1}$, $P_{99.9\_R51}$, and P_{50_R1} (Fig. 7). Fig. 7 also indicates that peak temperatures for P_{50_R1} and P_{50_R51} can occur at the ranges of 23.5–25.6 °C at station elevations below 110 m (DH, CH, HY, TQ, and TN), and 22.6–24.6 °C at stations with higher elevation (BK, CR, and NS). With regard to the behavior of extreme events ($P_{99.9}$) of heavy rain days (R_{51}) at each station, the peak temperatures vary from 23.5 °C at Ngan Son (NS) to 26.5 °C at Tuyen Quang (TQ). In addition, NS and Cho Ra (CR) stations, which are located at the same latitude, although NS differs in altitude (elevation of 650 m), have higher values of peak precipitation $P_{99.9\_R51}$ (255 mm at 23.5 °C) than CR (elevation of 165 m) does (209 mm at 24.6 °C). In general, higher-elevation stations have lower peak temperatures, except for Thai Nguyen (TN) station, which is located on hilly terrain known as a transiting region between delta and mountainous areas. Additionally, apart from TN (a Midland station), similar peak point temperatures and similar scaling trends are seen for both series $P_{99.9\_R1}$ and P_{50_R1} for the other stations.

4.2. PMP determination

4.2.1. Statistical method

In the Hershfield method, we selected the largest value of 24-hour precipitation for each year from 1962 to 2016 to obtain a series of annual extreme 24- hour rainfall at each station; the average value in each series ($\bar{R}_n$) varies from 94.3 mm at Cho Ra (CR) to 152.7 mm at Thai Nguyen (TN). The highest magnitude of 24-hour rainfall within each series (*Rmax*) at seven stations fluctuated from 211 mm (CR) to 375 mm (TN); the greatest value of *Rmax* was seen at Chiem Hoa station (506.1 mm). PMP determination results at eight meteorological stations are illustrated in Table 4 and Fig. 8. PMP, which was determined by the statistical method ($PMP_{\_statistic}$), varies from 232 mm (CR) to 895 mm (CH) with ratios between PMP and *Rmax* of less than 1.8 (from 1.07 at NS to 1.77 at CH); almost all stations obtain K_m values that are less than 5.7, apart from Chiem Hoa (CH – 12.78). The differences between *Rmax* and $\bar{R}_n$ at four stations (CR, NS, DH, and TN) range from 116.6 mm (124%) at Cho Ra (CR) to 223.4 mm (145%) at Thai Nguyen (TN). The outputs agree with the (*t-R*) relationship (Section 4.1), in which the scaling analysis of the 99.9th percentile for two datasets (R_1 and R_{51}) illustrates similar trends at those four stations (Fig. 7). It is in favor of the fact that among 36 events of 24-hour rainfall above 200 mm at the study site, there were 15 events at TN – a station with the highest value of $\bar{R}_n$ (152.7 mm). In addition, magnitudes of the largest rainfall (*Rmax*) at three stations (TQ, HY, and BK) are 191–211 mm (161–168%) higher than the average values of the data series $\bar{R}_n$; the difference between the apexes of the $P_{99.9\_R51}$ and $P_{99.9\_R1}$ scaling is 47–86 mm at the three aforementioned stations, at

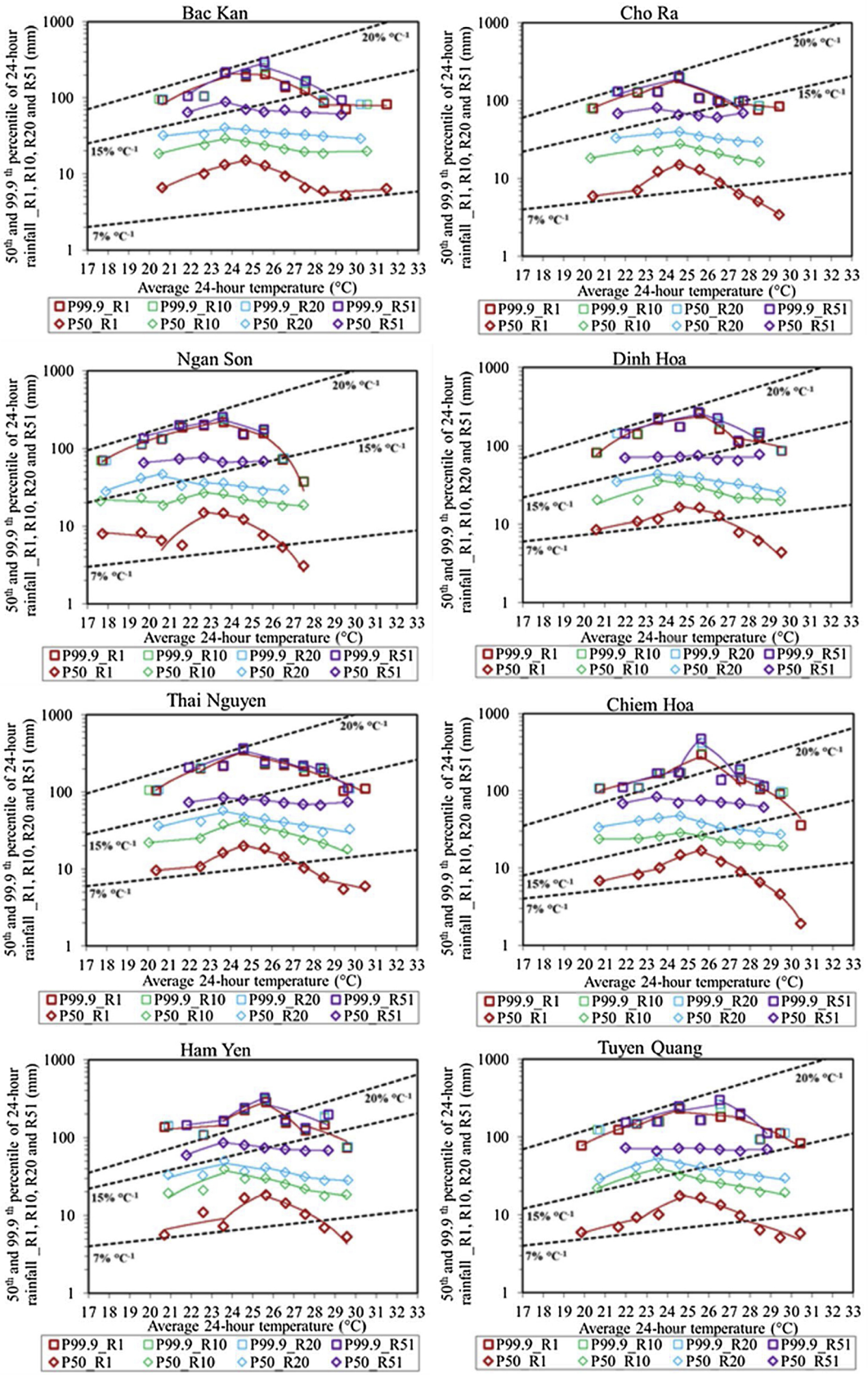

(caption on next page)

Fig. 7. The relationship between average 24-hour temperature and the 50th (P_{50}) and 99.9th ($P_{99.9}$) percentiles of 24-hour precipitation with the threshold of 1 mm (R_1), 10 mm (R_{10}), 20 mm (R_{20}), and 51 mm (R_{51}). The scaling rates are represented by dot black lines; the linear regressions within temperature ranges are shown in solid lines.

Table 4
PMP computation (mm).

Station	Elevation (m)	R_{max} (mm)	Statistical method		Moisture maximization method (PMP in mm using 4 options of t_d^{max})			
			K_m	PMP (mm)	t_{d_100}	t_{d_15d}	t_{d_30d}	t_{d_month}
BK	145	305	4.60	341	477	393	370	477
CR	165	211	4.48	232	301	237	260	281
NS	650	260	3.75	279	380	282	282	418
DH	105	276	3.78	296	407	340	342	407
TN	40	375	4.30	412	547	487	487	539
CH	60	506	12.78	895	682	571	645	694
HY	50	338	5.61	393	447	399	423	465
TQ	50	316	5.16	360	426	345	365	426

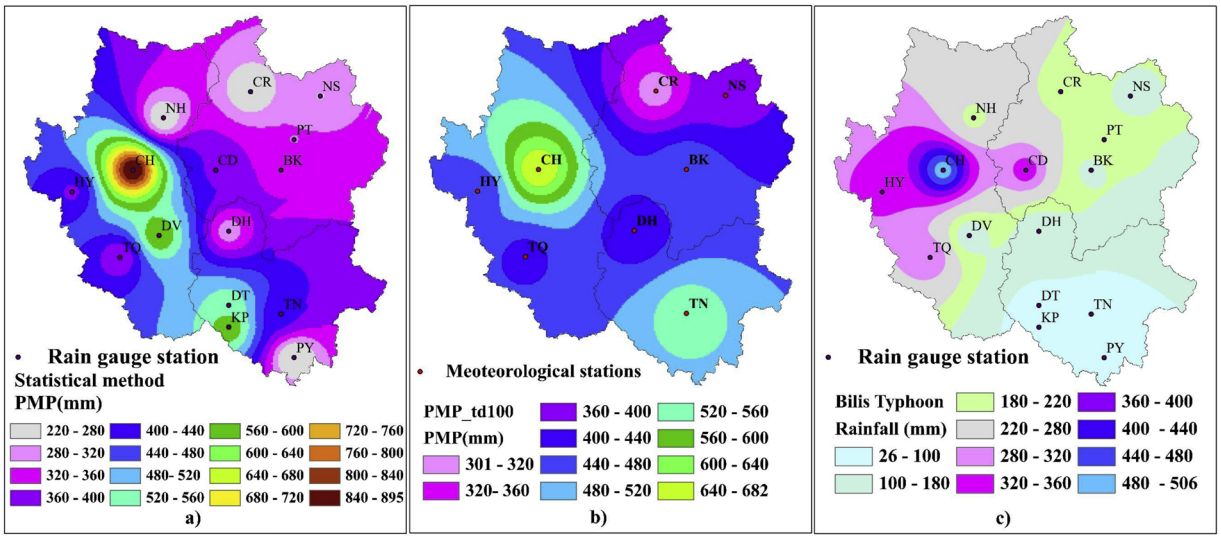

Fig. 8. Rainfall distribution regarding: a) Typhoon Bilis 2006; b) PMP_statistical method; c) PMP_moisture maximization method_t_{d_100}.

which the K_m ranges from 4.58 to 5.63. Interestingly, the peak value in the $P_{99.9}\_R_{51}$ scaling is 195 mm higher than the peak value in the $P_{99.9}\_R_1$ scaling at Chiem Hoa; this station also shows the greatest differences of 385 mm (318%) between *Rmax* and $\bar{R}_n$. It reveals that the most extreme precipitation *Rmax* of 506.1 mm at CH is significantly larger than values of the remaining data in the series of annual extreme 24-hour rainfall, in which the second highest rain amount at this station is 195.9 mm.

4.2.2. Moisture maximization method

PMPs are computed using precipitation, temperature, and relative humidity data associated with some of the largest rain events at eight meteorological stations over 55 years. From 1962–2016, the average number of days with rainfall amount above 200 mm at the study sites was 4.5 days (16 events at TN, 1 event at CR & CH, and 3–4 events at other stations). The computation of PMPs is thus implemented based on the five storm events, which were selected from the top five highest 24-hour precipitation amounts at each station. The maximum result at each station was selected as the PMP at that rain gauge.

In practice, precipitable water W_s was determined using temperature and relative humidity of the day of occurrence of extreme events and related to the station elevation. We calculated *Wmax* using to four options of dew point maximization using historical data, including t_d^{max} corresponding to the 100-year dew point (t_{d_100}), the largest value of $t_d max$ in a month (t_{d_month}), and maximum value within a window of 15 and 30 days (t_{d_15d} & t_{d_30d}) of a storm event. To evaluate the 100-year dew point temperatures (t_{d_100}) for each selected month, in which the top five highest 24-hour precipitation events occurred, we tested five distributions, namely the Gumbel (G), Normal (N), LogNormal (LN), Generalized Extreme Value (GEV) including maximum likelihood estimates (GEV1), and probability–weighted moment (GEV2) (Rousseau et al., 2014; Clavet-Gaumont et al., 2017). In order to determine the best fit, we conducted four goodness-of-fit (GOF) tests: the Chi-square test ($\chi 2$), Root mean square error (RMSE), Anderson-Darling test (A–D), and Kolmogorov-Smirnov test (K–S), with the support of the Comprehensive R Archive Network (CRAN) statistical packages

Table 5
GOF test of the best fit distribution.

Month	Best fit distribution (best scored result)				Highest-ranked distribution (sum of ranks)
	K-S test	A-D test	RMSE test	χ^2 test	
Bac Kan station (BK)					
9	N (0.033)	N (0.013)	GEV1 (0.974)	GEV2 (0.735)	GEV1&GEV2 (10)
8	N (0.019)	N (0.005)	GEV1 (0.962)	GEV2 (0.565)	LN (10)
7	N (0.019)	N (0.004)	GEV1 (3.123)	G (2.282)	GEV2 (8)
6	N (0.057)	N (0.017)	GEV1 (0.521)	GEV1 (0.631)	GEV2 (7)
Cho Ra station (CR)					
9	GEV1 (0.453)	GEV1 (0.520)	N (0.06)	N (0.008)	G (9)
7	GEV2 (0.323)	GEV2 (0.487)	GEV1 (0.073)	N (0.025)	G (8)
Ngan Son station (NS)					
9	GEV1 (0.453)	GEV1 (0.312)	N (0.079)	N (0.015)	G (9)
7	GEV1 (0.146)	GEV1 (0.313)	G (0.128)	G (0.035)	N (7)
6	GEV2 (0.765)	GEV2 (0.629)	G (0.155)	G (0.052)	N (7)
5	GEV2 (0.453)	GEV2 (0.488)	G (0.119)	G (0.032)	N&LN (11)
Dinh Hoa station (DH)					
10	G (0.765)	GEV1 (0.499)	LN (0.126)	GEV2 (0.032)	N (9)
8	GEV2 (0.765)	GEV1 (0.812)	LN (0.116)	LN (0.027)	N (8)
7	GEV2 (0.093)	N (0.253)	GEV2 (1.926)	G (0.273)	G&GEV1 (9)
Thai Nguyen station (TN)					
9	GEV2 (0.606)	GEV2 (0.579)	N (0.077)	LN (0.013)	G (10)
8	GEV1 (0.453)	GEV1 (0.466)	LN (0.097)	GEV1 (0.014)	N (9)
7	GEV2 (0.453)	GEV2 (0.265)	G (0.088)	G (0.015)	LN (10)
6	GEV1 (0.087)	GEV1 (0.094)	G (0.19)	G (0.074)	GEV2 (11)
Chiem Hoa station (CH)					
10	G (0.453)	G (0.374)	LN (0.13)	LN (0.037)	N (9)
9	GEV2 (0.221)	GEV2 (0.243)	LN (0.109)	GEV2 (0.024)	G&N (9)
7	GEV1 (0.323)	GEV1 (0.452)	LN (0.081)	LN (0.013)	N&GEV2 (11)
6	G (0.323)	G (0.307)	N (0.123)	N (0.031)	GEV1&GEV2 (9)
5	G (0.221)	G (0.274)	GEV1 (0.2)	GEV1 (0.162)	N&LN (10)
Ham Yen station (HY)					
7	GEV1 (0.606)	GEV2 (0.508)	LN (0.079)	LN (0.012)	N (10)
6	GEV2 (0.606)	GEV2 (0.4)	LN (0.062)	LN (0.008)	N (10)
5	GEV1 (0.453)	GEV2 (0.586)	N (0.097)	N (0.019)	G (8)
Tuyen Quang station (TQ)					
7	N (0.221)	N (0.133)	G (0.341)	G (0.224)	GEV1&GEV2 (8)
6	N (0.429)	N (0.281)	G (0.184)	G (0.065)	GEV1&GEV2 (8)
5	GEV1 (0.61)	N (0.502)	G (0.199)	G (0.079)	GEV2 (9)

(Gilleland and Katz, 2016; Scholz and Zhu, 2018). The GOF results are listed in Table 5. The best distribution for each month of each station was obtained from the smallest GOF result among the aforementioned distributions. Additionally, the lowest ranking score, which referred to the summary of each distribution's ranking results regarding each GOF, was represented as the selected distribution for each month at each station. In summary, the GEV2 (probability-weighted moment estimator) fits BK and TQ; the Normal distribution performed well at four stations (NS, DH, CH, and HY); Cho Ra station data is represented with the Gumbel distribution. However, at the Thai Nguyen station, a transition location between delta and mountain region, each month has a specific distribution. The selected distribution at each station (except TN) and selected distribution of each month at TN station were used to evaluate the 100-year dew point temperature for moisture maximization. Among the four approaches used to determine $t_d max$, the t_{d_100} and t_{d_month} produce large PMPs compared to the other two options, i.e., t_{d_15d} and t_{d_30d} (Table 4). PMP values using the 100-year dew point option for moisture maximization at the study site are introduced in Fig. 8b) & Fig. 8c).

The distributions of PMPs in the study area based on the two calculation methods have similar overall trends, especially in the western region including the Tuyen Quang province and CR station in the Bac Kan province. The statistical and moisture maximization methods both produced decreased PMPs towards the southwest–northeast direction in the upper part of the study site. In addition, Fig. 8. a) illustrates the distribution of heavy rain in the study area given the influence of typhoon Bilis (2006), which resulted in the most extreme 24-hour precipitation (*Rmax*) at CR, CH, HY, and TQ stations (Section 2.1). Because the Bilis typhoon had direct impacts on the South China region, at the study site, the rainfall intensity from this typhoon reduced that of the northwest (CH) to the southeast (TN) regions. However, the PMP magnitudes obtained from two methods show the decrease in distribution towards the southeast–northwest direction in the lower part of the study area (Thai Nguyen province and the south region of Bac Kan province). The result, therefore, depicts the great influence of terrain condition and typhoons direction or local atmospheric conditions on the distribution of extreme precipitation.

4.3. Future PMP estimation

Regarding WMO guideline (WMO, 2009a), PMP is defined as "the theoretical maximum precipitation for a given duration under

modern meteorological conditions … with no allowance made for long-term climatic trends". However, in Section 1.8, WMO also points out that in the 21st century it is likely to obtain the increase in the most extreme rainfall events as a result of the overall rise of moisture availability in a warming climate. Depth-area curves, moisture availability, storm efficiency, storm types, and generalized rainfall depths are therefore considered important factors in assessing the possible influence of climate change on PMP.

According to two GCM models and an RCM, we computed the average differences between corrected temperature using the variance scaling method ($T^{correct}_{model,i}$) and observation data (T_{obs}) within the baseline 1971–2000 using RMSE, as illustrated in Eq.(6).

$$RMSE_i = \sqrt{\frac{1}{N}\sum_{i=1}^{N}(T^{correct}_{model,i,j} - T_{obs,i,j})^2} \quad (6)$$

where $RMSE_i$ refers to Root Mean Square error of daily temperature in the i^{th} month (°C). $T^{correct}_{model,i,j}$ represents the corrected temperature of the model on the j^{th} day of the i^{th} month (°C). $T_{obs,i,j}$ illustrates observed temperature on the j^{th} day of the i^{th} month (°C). The average value of *RMSE* within 12 months for corrected MIROC 5, MRI, and HaG at eight stations is (3.24–3.47) °C, (3.29–3.54) °C, and (3.20–3.45) °C, respectively. The projection temperatures in each target year (2050 and 2080) for representative concentration pathways (RCP4.5 and RCP8.5) corrected by the variance scaling method are illustrated in Fig. 9. Comparing to historical data (1971–2000), an average monthly temperature at the study site regarding the GCM data is predicted to rise by (0.82–1.38) °C and (1.16–2.86) °C by the years 2050 and 2080, respectively; RCM data generates an increase of (1.41–1.63) °C in 2050 and (1.96–3.22) °C in 2080. In addition, HaG model produces higher projected temperatures than those of MIROC 5 in July and August by the year 2050 (1.05 °C) and 2080 (1.72 °C), respectively; similar trends are illustrated in the remaining 10 months.

The series of 24-hour precipitation of above 200 mm at the study site illustrates that the temperature varies from 21.5 °C to 28.5 °C, and relative humidity ranges from 85% to 99% (Fig. 4. b). The most extreme rainfall event at CR (506.1 mm) occurred at considerably high *RH* (98%) and temperature (25.9 °C) when compared to other precipitation events (from 250 mm to 400 mm). It is also predicted that there will be a rise in air moisture availability at high temperature, which can lead to a higher probability of more extreme precipitation events (Fig. 4. b).

In order to evaluate future scenarios of moisture maximization, the possible maximum dew point temperature in the future was determined based on the rise in air temperature and relative humidity. Future dew point determination can be computed based on future daily average air temperature and relative humidity (Lee et al., 2016), or scenarios of a future rise in air temperature and sea surface temperature and maximum relative humidity of 100% (Lee et al., 2017). Despite a fact that the Northern region is located in a humid subtropical climate, the monsoon system in relation to the variety of topographical relief results in the variation of climate from place to place. During the rainy season, southwesterly summer monsoon, tropical cyclones from the East Sea and tropical disturbances are some contributors to copious rains (Nguyen-Le et al., 2014; Do et al., 2016). The Asian summer monsoon performs a critically important role in precipitation supply and moisture transport from the Indian Ocean to the Indochina peninsula; while the western Pacific sub-tropical ridge fully dominates, this area often has hot, dry, and sunny weather (Nguyen-Le et al., 2014). It is also noted that the increase in air temperature itself could lead to a decrease in relative humidity. To evaluate the relationship between relative humidity and temperature (*RH˜t*), we applied the binning method with the same-bin width approach. The highest value of *RH* within each bin width of 0.1 °C in the (*RH˜t*) analysis was selected to evaluate the maximum relative humidity *(RHmax)* at that temperature bin (Fig. 10. a)). Regarding Fig. 10. a), the *RHmax* at eight stations experienced declining trends associated with the rise in temperature at a threshold range of 23–26 °C– a peak temperature in scaling analysis of extreme precipitation. Therefore, in this paper, a larger value of *RHmax* at higher temperature was selected as an upper boundary of *RH* at that temperature (points in Fig. 10. b)). The impact of station elevation on the (*RHmax˜t*) is also indicated in Fig. 10. b). The upper boundary of (*RHmax ˜t*) is therefore divided into three main types based on station elevations (z): i) z < 100 m (TN, HY, TQ, CH), ii) 100 m ≤ z < 150 m (DH, BK), and iii) z ≥ 150 m (CR, NS). For the relative humidity future scenario, the possible value of *RH* is determined based on projected temperature and upper boundary *RHmax* (*RHmax˜t*) regarding the three main above elevation classes.

RCP scenarios are described in Fig. 11. There is a rise in projected temperature regarding two GCMs and one RCM for two RCPs at the study site. In addition to the critical condition of relative humidity at high temperature (*RHmax˜t*), PMP would, therefore, increase in the future.

5. Discussion

5.1. Precipitation and temperature scaling analysis

The peak structure of scaling analysis in the study area (21°–22 °N) is suitable for the condition of mid-latitude regions (from 20°–55° S and N) (Utsumi et al., 2011). The differences between R_{51} and R_1 lines can show the role of extreme events in a dataset. The extreme precipitation analysis depends on the rainfall threshold because small intensities of precipitation strongly affect the percentile computation. As illustrated in Figs. 6 and 7, the $P_{99.9}R_{51}$, which is not influenced by the small magnitude of precipitation, presents greater values of extreme events than the $P_{99.9}R_1$ does. It is also noted that seasonal selection may affect the scaling trend. At this study site, heavy rain events are often associated with the occurrences of tropical typhoons and storms during the rainy season from May to October (MO), though downpour sometimes occurs in April due to troughs. According to $P_{99.9}R_1$ analysis (Fig. 6), a temperature of 18.6 °C experiences the second hump in the April to October (AO) dataset; a slightly stable trend is illustrated within a temperature range of 17.6–19.6 °C in the MO dataset. When excluding April data, $P_{99.9}R_{1\_MO}$ (from May to October) is lower than $P_{99.9}R_{1\_AO}$ (from April to October) at the temperature below 19.5 °C. In both cases, 19.5 °C can be considered a transition temperature

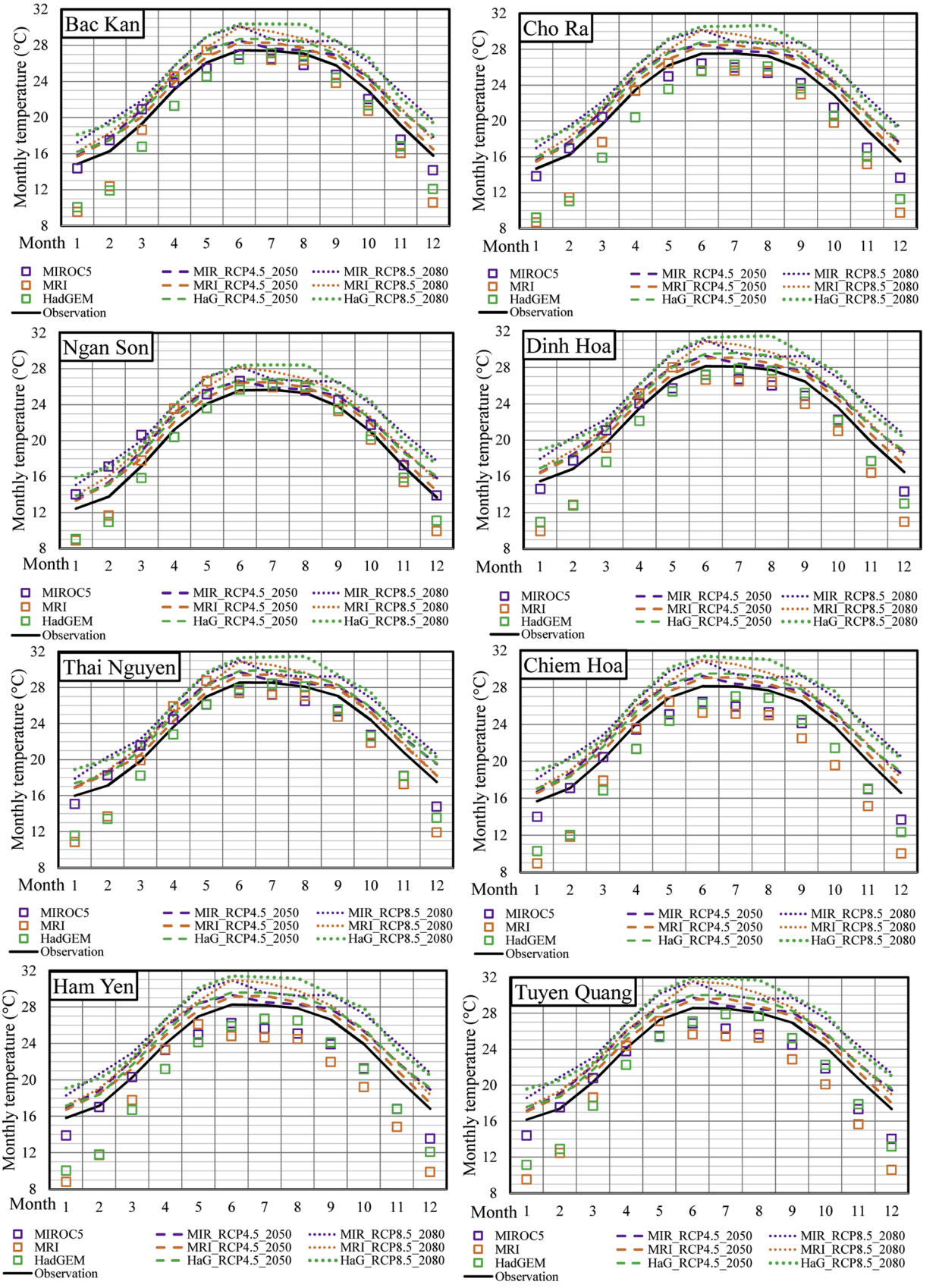

(caption on next page)

Fig. 9. Monthly temperature: Points refer to historical output (1971–2000) from MIROC5 (MIR), MRI-CGCM3 (MRI), and HadGEM3-RA (HaG). Projected monthly temperature after correction by variance scaling method in RCP4.5_2050 and RCP8.5_2080 are represented in dash lines and dot lines, respectively; monthly observation temperature is shown in black solid line.

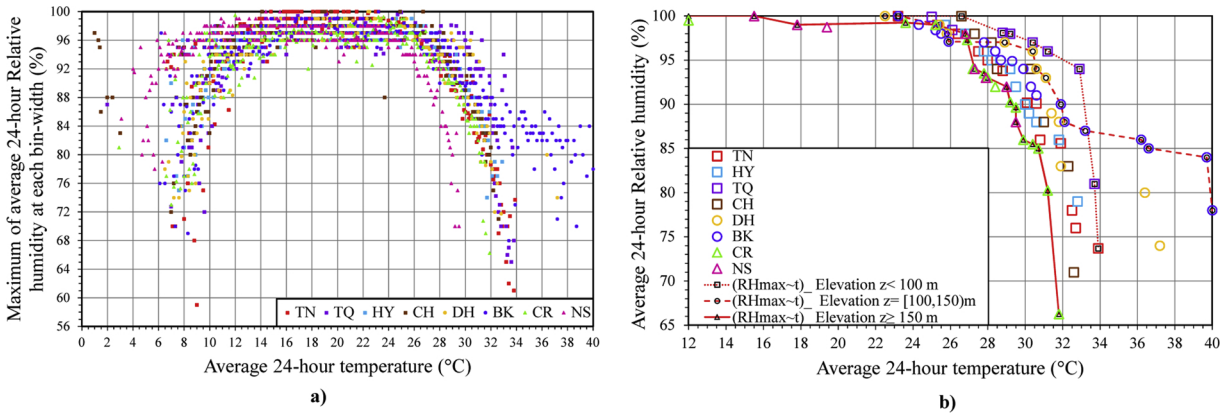

Fig. 10. Characteristic of Relative Humidity a) Maximum of average 24-hour relative humidity (*RHmax*) within each temperature bin width at each station; b) Points illustrate observed *RHmax* at high temperatures at each station, lines represent upper boundary of *RHmax* at the group of stations with respect to elevations.

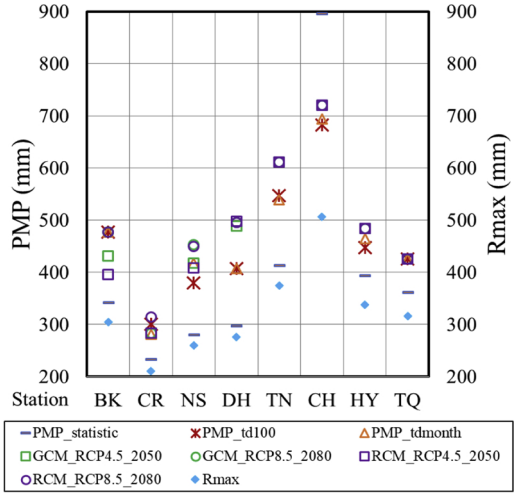

Fig. 11. PMP calculation with respect to historical data as well as GCM_RCP and RCM_RCP approaches.

when it provides a starting point for the second rise of the trend lines. Comparatively similar tendencies are seen at higher temperatures at the two datasets: including and excluding April.

For further evaluation of scaling analysis, we also set up the relationship between average 24-hour temperature and heavy precipitation (R_{10}) and very heavy precipitation (R_{20}) (WMO, 2009b). With regards to the 99.9th percentile ($P_{99.9}$) of selected events (R_1, R_{10}, R_{20}, and R_{51}), when the rainfall thresholds increase from 1 mm (R_1) to 51 mm (R_{51}) peak temperature at each station is stable at 23.5–25.6 °C, except for BK and TQ stations. There was a rise by 2 °C in peak temperature at BK (23.5–25.5 °C) and TQ (24.5–26.5 °C) (Fig. 7). Interestingly, with respect to the 50th percentile determination for four options of rainfall thresholds (R_1, R_{10}, R_{20}, and R_{51}), when the magnitudes rise from R_1 to R_{51}, peak temperatures decline by 1 °C at three stations in the mountainous region (NS, CR, and BK) and at TN station, and 2 °C at two midland stations (CH and HY). A stable temperature of 24.6 °C is seen at TQ; DH is the only station that experiences an increase of 0.9 °C (24.6–25.5 °C). In addition, the scaling rates of 10% per degree Celsius for $P_{50}R_{20}$ and $P_{50}R_{10}$ are shown at two stations, namely CR and CH, while the six remaining stations experienced a rate of from 15 to 20% per degree Celsius. According to Fig. 7, the 50th percentile rainfall temperature scale values are lower than the 99.9th percentile scaling values. The rise of scaling analysis associated with the rise of percentile may reveal that the temperature sensitivity for more extreme precipitation (99.9th percentile of 24-hour rainfall) is higher than that for average extreme rainfall events (50th percentile of 24-hour rainfall). It also implies that fully saturated conditions are likely to be present at more extreme precipitation events (Lenderink et al., 2010; Herath et al., 2018).

Table 6a
The range of slope between the logarithm of rainfall and average 24-hour temperature using linear regression in regard to temperature ranges for the 99.9th ($P_{99.9}$) and 50 th (P_{50}) percentiles of rainfall events (R_1, R_{10}, R_{20}, and R_{51}). Values in brackets illustrate the lowest and highest magnitudes of minimum and maximum slope values [(log mm) /°C] within the temperature ranges at 8 stations.

	Temperature range (°C)			
	17.5 ÷ 20 °C	20 ÷ 22 °C	22 ÷ 24 °C	24 ÷ 27 °C
$P_{99.9}\_R_1$	[0.086, 0.107]	[0.059, 0.138]	[0.059, 0.139]	[0.037, 0.139]
$P_{99.9}\_R_{51}$	[0.064, 0.064]	[0.033, 0.123]	[0.033, 0.147]	[0.038, 0.218]
$P_{50}\_R_1$	[0.024, 0.067]	[0.024, 0.175]	[0.057, 0.193]	[0.088, 0.193]
$P_{50}\_R_{10}$	[0.024, 0.024]	[0.003, 0.105]	[0.038, 0.105]	[0.038, 0.104]
$P_{50}\_R_{20}$	[0.082, 0.082]	[0.006, 0.095]	[0.026, 0.170]	[0.026, 0.039]
$P_{50}\_R_{51}$	[0.025, 0.025]	[0.004, 0.091]	[0.004, 0.091]	[0.007, 0.038]

In addition, we also evaluated the relationship between the logarithm of 24-hour precipitation (log(R)) and temperature (t) using linear regression in regard to the 99.9th ($P_{99.9}$) and 50th (P_{50}) percentiles of rainfall events (R_1, R_{10}, R_{20}, and R_{51}). In general, the $P_{99.9}\_R_{51}$ has peak slope values (from 0.038 (TQ) to 0.218 (DH)) within 24–27 °C; a range of regression slope from 0.059 (CH) to 0.139 (HY) is generated at 22–24 °C relation to $P_{99}\_R_1$. With regard to the 50th percentile, when the rainfall thresholds increase from 1 mm to 51 mm, there is a decrease in the temperature range, which experiences a higher magnitude of linear slopes (Table 6a). For example, regarding to $P_{50}\_R_1$, a maximum slope of 0.193 [(log mm) /°C] is shown at 22–26 °C; $P_{50}\_R_{51}$ has the largest slope of 0.091 [(log mm) /°C] at temperature from 20 to 24 °C. With respect to the 50th percentile at each station, the largest slope values also decrease when rainfall threshold varies from R_1 to R_{51} (Table 6b).

5.2. PMP and climate change

In general, the PMP computation corresponding to the 100-year maximum t_d in a storm event month are in good agreement with PMP_RCP4.5 in 2050 and 2080. Compared to historical data calculations, the projected computations of PMP of GCMs and RCM provide larger magnitudes of PMPs for RCP8.5, especially in 2080. Such rises occur at DH for RCM in 2050 (24.5%), GCM in 2080 (21.7%), and at NS in 2080 (8.4% for GCM and 7.7% for RCM). In the future climate model approach, regarding stabilization scenario (RCP4.5), PMP calculations at all stations are relatively stable for the two target years 2050 and 2080. There are moderate differences between historical data calculations and projected computation of PMP for RCP8.5 scenarios in the two target years, especially in 2080.

6. Conclusion

This study aims to assess the precipitation variation characteristics in northeast Vietnam by identifying the relationship between extreme 24-hour rainfall and average 24-hour temperature. The study also estimated the 24-hour probable maximum precipitation in the study area highlighting the possible impacts of warming climate on extreme rain and PMP.

Results from scaling analysis of precipitation and temperature are suitable according to recent analysis (Berg et al., 2009; Hardwick Jones et al., 2010; Utsumi et al., 2011; Rousseau et al., 2014) such as the CC-like rate at low temperature, super CC-rate at high temperature, and the peak-like structure at mid-latitudes. It also presents the effect of a time scale as well as the sensitive behavior of extreme rainfall towards temperatures when compared to the average approach. The relationship between relative humidity and temperature reflects a similar trend in the scaling analysis (same peak temperature of 25–26 °C).

While the statistical method focuses only on the behavior of extreme rainfall events in historical data, PMP results from the moisture maximization method, which is based on the relationship with other meteorological parameters such as humidity and temperature and can be utilized in the further study, especially in the context of a warming climate. With a projected rise in temperature, especially for RCP8.5, PMP is predicted to increase by the years 2050 and 2080. Additionally, the spatial distribution of

Table 6b
Maximum values of slope between logarithm of rainfall and average 24-hour temperature using linear regression at each station regard to the 99.9th ($P_{99.9}$) and 50th (P_{50}) percentiles of rainfall events (R_1, R_{10}, R_{20}, and R_{51}).

	Station							
	BK	CR	NS	DH	TN	CH	HY	TQ
$P_{99.9}\_R_1$	0.102	0.089	0.086	0.138	0.112	0.121	0.139	0.107
$P_{99.9}\_R_{51}$	0.114	0.060	0.108	0.218	0.084	0.213	0.147	0.077
$P_{50}\_R_1$	0.092	0.159	0.175	0.088	0.128	0.109	0.193	0.132
$P_{50}\_R_{10}$	0.062	0.044	0.080	0.072	0.104	0.038	0.105	0.086
$P_{50}\_R_{20}$	0.085	0.026	0.082	0.051	0.133	0.039	0.170	0.095
$P_{50}\_R_{51}$	0.077	0.038	0.025	0.019	0.039	0.052	0.091	0.038

PMPs based on moisture maximization using 100-year dew point, which refers to the most extreme rainfall events that possibly occur at a study area, can be used in evaluating rain-induce problems, such as floods or landslide.

Since statistical records are not available for public access, lacking historical data has become one of the biggest difficulties for researchers in Vietnam. Findings from this paper thus provide as an initial approach in evaluating extreme precipitation in this northeast region in cases where full meteorological data records arelacking. Nevertheless, there are limitations in this study, such as the sole application of 24-hour precipitation and air surface temperature to evaluate the CC scaling. Whilst the hypothesis of this scaling analysis only considers the intensity of rain events as a conditional factor for rainfall occurrence (Hardwick Jones et al., 2010), other governing factors such as sources of moisture regarding shorter durations like 1 to 6 h should be taken into further studies.

According to the PMP determination methods, the occurrence of extreme precipitation often depends on many factors, including moisture availability, wind speed and direction, temperature, and topography condition; the statistical method, which only focuses on the variation of extreme precipitation, reveals shortcomings. PMPs derived from the Hershfield method tend to vary with changes in the size of annual extreme precipitation. For example, compared to the outputs resulting from 55-year data (1962–2016), the application of rain records from 1961 to 2016 at TQ brings about a rise of 1.11 and 0.33 mm in the average and standard deviation values, respectively. The statistical variable K_m (frequency factor) declines by 0.13; the PMP also decreases from 363.34 mm (55-year data) to 360.38 mm (56-year data). In addition, it is a fact that the spatial distribution of extreme rainfall is strongly affected by the orographic condition of the basin. However, the terrain features were neglected in the computation of moisture maximization approach in this paper. The moisture maximization method, which considers significant roles of available moisture in the occurrence of extreme rainfall, also reveals some uncertainties, such as in the procedure of determining maximum precipitable water (*Wmax*) concerning the maximum dewpoint temperature $t_d max$. In cases retrieving $t_d max$ within a 15-day and 30-day windows regarding the date of a storm (t_{d_15d} and t_{d_30d}), the vapor water holding capacity of the atmosphere would decline when the condensation formation often leads to a decrease in the air temperature. When the maximum dewpoint temperature is selected from the time series of annual maximum dewpoint (t_{d_100} and t_{d_month}) in the month that a storm occurs, it is likely to obtain the series in a period that is warmer than that during the storm occurrence date. Since the precipitable water tends to rise with air temperature as described in the Clausius-Clapeyron equation, large maximization ratios would lead to higher PMPs (as discussed in Section 4.2.2). Moreover, the paper utilized the average dewpoint temperature rather than 12-hour persisting values to represent the storm moisture; it, therefore, would lead to the uncertainty of exaggeration in PMP values. This article also based on the recommendations of the WMO guideline (WMO, 2017) in applying the 30-year standard normal to assess climatological surface parameters such as air surface temperature. The basic assumption of stationary climate assumes that the climate is variable; however, the variations' properties are considered to be constant with time (WMO, 2009b). This application of a stationary climate would disregard climate change, which can alter the variability and extremes of weather variables (Nathan et al., 2016). Comparisons with non-stationary analyses of extreme weather variables are therefore necessary for future researches. Significant errors in the climate models in addition to the downscale method also would lead to uncertainties in the evaluation of future temperature at the study site. Whilst the PMP determination focused on the high magnitude of daily projected temperature, the predicted trend of PMPs under the rise of air temperature was evaluated to a certain extent.

Conflicts of interests

The authors declare no conflict of interest.

Acknowledgements

This research was supported by the Vietnamese Government scholarship (project 911) and the Social Implementation Program on Climate Change Adaptation Technology (SI-CAT) of MEXT, Japan. We acknowledge the World Climate Research Programme's Working Group on Coupled Modelling and the Coordinated Regional Climate Downscaling Experiment – CORDEX in East Asia for GCMs and RCMs data access; the Naval Meteorology & Oceanography Command and its portal – The Joint Typhoon Warning Center for historical typhoon data; the Vietnam Institute of Meteorology and Hydrology for meteorological data; the Climate Data Operators (CDO) for climate data analysis; and the R project and its packages for statistical computing. The authors would like to thank anonymous reviewers for their very constructive comments and suggestions that help to bring the manuscript to its present form.

Appendix A. Supplementary data

Supplementary material related to this article can be found, in the online version, at doi:https://doi.org/10.1016/j.ejrh.2019.100599.

References

Alduchov, O.A., Eskridge, R.E., 1996. Improved magnus form approximation of saturation vapor pressure. J. Appl. Meteorol. 35, 601–609. https://doi.org/10.1175/1520-0450(1996)035<0601:IMFAOS>2.0.CO;2.

Alias, N.E., Luo, P., Takara, K., 2013. Probable maximum precipitation using statistical method for the Yodo River Basin. J. Japan Soc. Civ. Eng. Hydraul. Eng. 69, 157–162. https://doi.org/10.2208/jscejhe.69.I.

Baek, H.J., Lee, J., Lee, H.S., Hyun, Y.K., Cho, C., Kwon, W.T., Marzin, C., Gan, S.Y., Kim, M.J., Choi, D.H., Lee, J., Lee, J., Boo, K.O., Kang, H.S., Byun, Y.H., 2013. Climate change in the 21st century simulated by HadGEM2-AO under representative concentration pathways. Asia-Pacific J. Atmos. Sci. 49, 603–618. https://doi.org/10.1007/s13143-013-0053-7.

Beauchamp, J., Leconte, R., Trudel, M., Brissette, F., 2013. Estimation of the summer-fall PMP and PMF of a northern watershed under a changed climate. Water Resour. Res. 49, 3852–3862. https://doi.org/10.1002/wrcr.20336.

Berg, P., Haerter, J.O., 2013. Unexpected increase in precipitation intensity with temperature - a result of mixing of precipitation types? Atmos. Res. 119, 56–61. https://doi.org/10.1016/j.atmosres.2011.05.012.

Berg, P., Haerter, J.O., Thejll, P., Piani, C., Hagemann, S., Christensen, J.H., 2009. Seasonal characteristics of the relationship between daily precipitation intensity and surface temperature. J. Geophys. Res. 114, 1–9. https://doi.org/10.1029/2009JD012008.

Berg, P., Moseley, C., Haerter, J.O., 2013. Strong increase in convective precipitation in response to higher temperature strong increase in convective precipitation in response to higher temperatures. Nat. Geosci. 6, 181–185. https://doi.org/10.1038/ngeo1731.

Boessenkool, B., Bürger, G., Heistermann, M., 2016. Effects of sample size on estimation of rainfall extremes at high temperatures. Nat. Hazards Earth Syst. Sci. Discuss. 1–11. https://doi.org/10.5194/nhess-2016-183.

Casas, M.C., Rodríguez, R., Prohom, M., Gázquez, A., Redaño, A., 2011. Estimation of the probable maximum precipitation in Barcelona (Spain). Int. J. Climatol. 31, 1322–1327. https://doi.org/10.1002/joc.2149.

Chen, J., Brissette, F.P., Chaumont, D., Braun, M., 2013. Finding appropriate bias correction methods in downscaling precipitation for hydrologic impact studies over North America. Water Resour. Res. 49, 4187–4205. https://doi.org/10.1002/wrcr.20331.

Chu, J., Levine, A., Daida, S., Schiber, D., Fukada, E., Sampson, C.R., 2017. Western North Pacific Ocean Best track data [WWW document]. Nav. Res. Lab Monterey Jt. Typhoon Warn. Cent. URL http://www.metoc.navy.mil/jtwc/jtwc.html?western-pacific (accessed 11.24.17).

Clavet-Gaumont, J., Huard, D., Frigon, A., Koenig, K., Slota, P., Rousseau, A., Klein, I., Thiémonge, N., Houdré, F., Perdikaris, J., Turcotte, R., Lafleur, J., Larouche, B., 2017. Probable maximum flood in a changing climate: an overview for Canadian basins. J. Hydrol. Reg. Stud. 13, 11–25. https://doi.org/10.1016/j.ejrh.2017.07.003.

Davies, T., Cullen, M.J.P., Malcolm, A.J., Mawson, M.H., Staniforth, A., White, A.A., Wood, N., 2005. A new dynamical core of the Met Office's global and regional modelling of the atmosphere. Q. J. R. Meteorol. Soc. 131, 1759–1782. https://doi.org/10.1256/qj.04.101.

Do, D.T., Hole, L.R., Tran, A.D., Hoang, D.C., Nguyen, B.T., 2016. Verification of forecast weather surface variables over Vietnam using the National numerical weather prediction system. Adv. Meteorol. 2016, 1–11. https://doi.org/10.1155/2016/8152413.

Fang, G.H., Yang, J., Chen, Y.N., Zammit, C., 2015. Comparing bias correction methods in downscaling meteorological variables for a hydrologic impact study in an arid area in China. Hydrol. Earth Syst. Sci. 19, 2547–2559. https://doi.org/10.5194/hess-19-2547-2015.

Gilleland, E., Katz, R., 2016. Extreme value analysis. J. Stat. Softw. 72, 1–39.

Hardwick Jones, R., Westra, S., Sharma, A., 2010. Observed relationships between extreme sub- daily precipitation, surface temperature, and relative humidity. Geophys. Res. Lett. 37, L22805. https://doi.org/10.1029/2010GL045081.

Hawkins, E., Osborne, T.M., Ho, C.K., Challinor, A.J., 2013. Calibration and bias correction of climate projections for crop modelling: an idealised case study over Europe. Agric. For. Meteorol. 170, 19–31. https://doi.org/10.1016/j.agrformet.2012.04.007.

Herath, M.S., Sarukkalige, R., Nguyen, V.T., Van, 2018. Evaluation of empirical relationships between extreme rainfall and daily maximum temperature in Australia. J. Hydrol. 556, 1171–1181. https://doi.org/10.1016/j.jhydrol.2017.01.060.

Hershfield, D.M., 1961. Estimation of the probable maximum precipitation. J. Hydraul. Div. 87, 99–116.

Hershfield, D.M., 1965. Method for estimating probable maximum rainfall. Am. Water Assoc. 57, 965–972. https://doi.org/10.1002/j.1551-8833.1965.tb01486.x.

IPCC, 2015. Climate change 2014: synthesis report. Contribution of working groups I, II and III to the Fifth assessment report of the intergovernmental panel on climate change. Intergov. Panel Clim. Change 169. https://doi.org/10.1017/CBO9781107415324.

Ishida, K., Ohara, N., Kavvas, M.L., Chen, Z.Q., Anderson, M.L., 2018. Impact of air temperature on physically-based maximum precipitation estimation through change in moisture holding capacity of air. J. Hydrol. 556, 1050–1063. https://doi.org/10.1016/j.jhydrol.2016.10.008.

Jakob, D., Walland, D., 2016. Variability and long-term change in Australian temperature and precipitation extremes. Weather Clim. Extrem. 14, 36–55. https://doi.org/10.1016/j.wace.2016.11.001.

Jothityangkoon, C., Hirunteeyakul, C., Boonrawd, K., Sivapalan, M., 2013. Assessing the impact of climate and land use changes on extreme floods in a large tropical catchment. J. Hydrol. 490, 88–105. https://doi.org/10.1016/j.jhydrol.2013.03.036.

Killick, R., Eckley, I., 2013. Changepoint: an R package for changepoint analysis. Lancaster Univ. 58, 1–15. https://doi.org/10.1359/JBMR.0301229.

Killick, R., Eckley, I., 2016. Changepoint: An R Package for Changepoint Analysis. R Packag. Version 2.2.2. pp. 1–28.

Kunkel, K.E., Karl, T.R., Easterling, D.R., Redmond, K., Young, J., Yin, X., Hennon, P., 2013. Probable maximum precipitation and climate change. Geophys. Res. Lett. 40, 1402–1408. https://doi.org/10.1002/grl.50334.

Lawrence, M.G., Planck, M., 2005. The relationship between relative humidity and the dewpoint temperature in moist air: a simple conversion and applications. Bull. Am. Meteorol. Soc. 86, 225–233. https://doi.org/10.1175/BAMS-86-2-225.

Le, Q.H., Nguyen, T.H.Van, Pham, V.S., 2014. Landslide inventory mapping in fourteen northern provinces of Vietnam: achievements and difficulties. Adv. Cult. Living Landslides 1, 501–509. https://doi.org/10.1007/978-3-319-59469-9.

Lee, O., Park, Y., Kim, E.S., Kim, S., 2016. Projection of Korean probable maximum precipitation under future climate change scenarios. Adv. Meteorol. 2016, 1–16. https://doi.org/10.1155/2016/3818236.

Lee, J., Choi, J., Lee, O., Yoon, J., Kim, S., 2017. Estimation of probable maximum precipitation in Korea using a regional climate model. Water 9, 1–12. https://doi.org/10.3390/w9040240.

Lenderink, G., Meijgaard, E., Van, 2010. Linking changes in hourly precipitation extremes to the Clausius-Clapeyron relation. Geophys. Res. Lett. 37, 39–43.

Lenderink, G., Mok, H.Y., Lee, T.C., Van Oldenborgh, G.J., 2011. Scaling and trends of hourly precipitation extremes in two different climate zones - Hong Kong and the Netherlands. Hydrol. Earth Syst. Sci. 15, 3033–3041. https://doi.org/10.5194/hess-15-3033-2011.

Micovic, Z., Schaefer, M.G., Taylor, G.H., 2015. Uncertainty analysis for probable maximum precipitation estimates. J. Hydrol. 521, 360–373. https://doi.org/10.1016/j.jhydrol.2014.12.033.

MONRE, 2016. Climate change and sea level rise scenarios for Vietnam. Minist. Nat. Resour. Environ. Vietnam 188.

Nathan, R., Jordan, P., Scorah, M., Lang, S., Kuczera, G., Schaefer, M., Weinmann, E., 2016. Estimating the exceedance probability of extreme rainfalls up to the probable maximum precipitation. J. Hydrol. 543, 706–720. https://doi.org/10.1016/j.jhydrol.2016.10.044.

Nguyen-Le, D., Matsumoto, J., Ngo-Duc, T., 2014. Climatological onset date of summer monsoon in Vietnam. Int. J. Climatol. 34, 3237–3250. https://doi.org/10.1002/joc.3908.

Panthou, G., Mailhot, A., Laurence, E., Talbot, G., 2014. Relationship between surface temperature and extreme rainfalls : a multi-time-scale and event-based analysis. Am. Meteorol. Soc. 1, 1999–2011. https://doi.org/10.1175/JHM-D-14-0020.1.

Pierce, D.W., Cayan, D.R., Maurer, E.P., Abatzoglou, J.T., Hegewisch, K.C., 2015. Improved bias correction techniques for hydrological simulations of climate change. J. Hydrometeorol. 16, 2421–2442. https://doi.org/10.1175/JHM-D-14-0236.1.

Rastogi, D., Shih-Chieh, K., Moetasim, A., Mei, R., Kabela, E.D., Gangrade, S.S., Preston, N.B., Singh, B.L., Anantharaj, N., V.G, 2017. Effects of climate change on probable maximum precipitation: a sensitivity study over the Alabama-Coosa-Tallapoosa River Basin. J. Geophys. Res. Atmos. 122, 4808–4828. https://doi.org/10.1002/2016JD026001.

Rousseau, A.N., Klein, I.M., Freudiger, D., Gagnon, P., Frigon, A., Ratté-fortin, C., 2014. Development of a methodology to evaluate probable maximum precipitation (PMP) under changing climate conditions : application to southern Quebec, Canada. J. Hydrol. 519, 3094–3109. https://doi.org/10.1016/j.jhydrol.2014.10.053.

Scholz, F., Zhu, A., 2018. K-Sample Rank Tests and Their Combinations. R Packag. Version 1.2-8 34.

Schulzweida, U., 2018. Climate data operators (CDO) user Guide, version 1.9.4. MPI Meteorol. 1–215.

Shin, Y., Takara, K., Ostric, M., 2013. Depth-Area-duration analysis in a Korean River Basin. J. Japan Soc. Civ. Eng. 69, 151–156. https://doi.org/10.2208/jscejhe.69.I_

151.
Terink, W., Hurkmans, R.T.W.L., Torfs, P.J.J.F., Uijlenhoet, R., 2009. Bias correction of temperature and precipitation data for regional climate model application to the Rhine basin. Hydrol. Earth Syst. Sci. Discuss. 6, 5377–5413. https://doi.org/10.5194/hess-14-687-2010.
Terink, W., Hurkmans, R.T.W.L., Torfs, P.J.J.F., Uijlenhoet, R., 2010. Evaluation of a bias correction method applied to downscaled precipitation and temperature reanalysis data for the Rhine basin. Hydrol. Earth Syst. Sci. 14, 687–703. https://doi.org/10.5194/hess-14-687-2010.
Teutschbein, C., Seibert, J., 2012. Bias correction of regional climate model simulations for hydrological climate-change impact studies: review and evaluation of different methods. J. Hydrol. 456–457, 12–29. https://doi.org/10.1016/j.jhydrol.2012.05.052.
Toure Halimatou, A., Kalifa, T.N.K.-B., 2017. Assessment of changing trends of daily precipitation and temperature extremes in Bamako and S egou in Mali from 1961-2014 tour. Weather Clim. Extrem. 1–9. https://doi.org/10.1016/j.wace.2017.09.002.
Utsumi, N., Seto, S., Kanae, S., Maeda, E.E., Oki, T., 2011. Does higher surface temperature intensify extreme precipitation? Geophys. Res. Lett. 38, 1–5. https://doi.org/10.1029/2011GL048426.
Vietnam Standard, 2015. TCVN 10406:2015 - Hydraulic Structures - Calculation of Design Drainage Coefficient 49.
Watanabe, M., Suzuki, T., O'Ishi, R., Komuro, Y., Watanabe, S., Emori, S., Takemura, T., Chikira, M., Ogura, T., Sekiguchi, M., Takata, K., Yamazaki, D., Yokohata, T., Nozawa, T., Hasumi, H., Tatebe, H., Kimoto, M., 2010. Improved climate simulation by MIROC5: mean states, variability, and climate sensitivity. J. Clim. 23, 6312–6335. https://doi.org/10.1175/2010JCLI3679.1.
WMO, 1969. Manual for depth-Area-duration analysis of storm precipitation. World Meteorol. Organ. 131.
WMO, 2009a. Manual on estimation of probable maximum precipitation (PMP). World Meteorol. Organ. 291.
WMO, 2009b. Climate data and monitoring - guidelines on analysis of extremes in a changing climate in support of informed decisions for adaptation. World Meteorol. Organ. 55.
WMO, 2017. WMO guidelines on the calculation of climate normals. World Meteorol. Organ. 29.
Yukimoto, S., Adachi, Y., Hosaka, M., Sakami, T., Yoshimura, H., Hirabara, M., Tanaka, T.Y., Shindo, E., Tsujino, H., Deushi, M., Mizuta, R., Yabu, S., Obata, A., Nakano, H., Koshiro, T., Ose, T., Kitoh, A., 2012. A New global climate model of the meteorological research institute: MRI-CGCM3 -model description and basic performance-. J. Meteorol. Soc. Japan 90A, 23–64. https://doi.org/10.2151/jmsj.2012-A02.